Raman, Conventional Infrared and Synchrotron Infrared Spectroscopy in Mineralogy and Geochemistry: Basics and Applications

Biliana Gasharova

ANKA Synchrotron Light Source / Institute for Synchrotron Radiation, Research Center Karlsruhe, P.O. Box 3640, 76021 Karlsruhe, Germany

Both vibrational spectroscopy methods, Raman and infrared (IR), have proved a useful tool for fingerprint analysis, structural characterization, *in-situ* monitoring of reaction kinetics / pressure / temperature dependence, quantitative analysis, as a probe of interatomic forces, and for calculation of thermodynamic and elastic properties. Over the past decades the development of microbeam techniques has had a major impact on vibrational studies and thus these techniques are enjoying a growing popularity in the geosciences. As with any experimental approach some theoretical understanding of the physical phenomena underlying the experiment as well as some knowledge about the principles and performance of the instrumentation are essential for a meaningful analysis of vibrational spectra. Examples of applications of Raman and IR spectroscopy in mineralogy and geochemistry will follow a brief introduction to the basics of both methods and the corresponding instrumentation.

They are number of excellent summaries of both theory and applications available in the literature. For example, books as those of Nakamoto (1996, first published in 1963) describing fundamental theories of vibrational spectroscopy and illustrating their applications to inorganic and coordination compounds; Farmer (1974) providing an excellent description of theory, instrumentation and techniques related to mineralogy along with very extensive and valuable summary of vibrational studies across all mineralogical fields; Hawthorne (1988) summarizing theory and applications in mineralogy and geology. Some more recent books of interest could be Mirabella (1992), Putnis (1995), Turell and Corset (1996), McCreery (2000), Chalmers and Griffiths

(2001), Beran and Libowitzky (2004). The content of the theoretical part in this article is based on the literature mentioned above, which has not been further cited throughout the text.

Spectroscopic methods

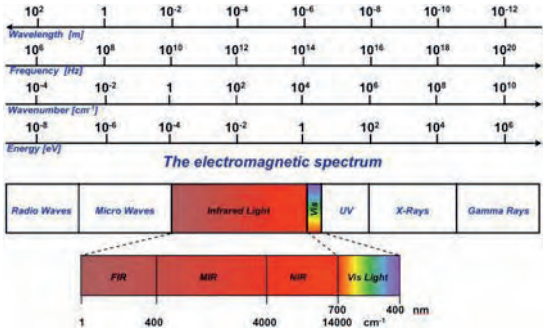

FIGURE 1. Regions of the EM spectrum with ΔE indicated in eV (energy), cm^{-1} (wavenumber), Hz (frequency) and m (wavelength).

Spectroscopic methods are complementary techniques or some times even an alternative to the traditionally applied diffraction methods. In terms of the interaction of radiation with matter, diffraction involves a change in direction of the incident radiation, without change in its energy.

The determination of structure by diffraction depends largely on the periodicity of the structure and therefore produces a long-range or average picture. Spectroscopic methods on the other hand provide information about the local structure of a material like local chemical and crystallographic environment, coordination number, site symmetry, etc. and do not depend on long-range periodicity or crystallinity.

Although there are many different spectroscopic methods they all work on the same basic principle. Under some conditions, an incident beam of radiation can be absorbed, transmitted, reflected or scattered by matter, or alternatively, can cause the emission of radiation from the material. The energy differences between ground and excited states cover the entire range of the EM spectrum from radio frequency (~10^6 Hz) to x-ray and g-ray frequencies (up to ~10^{20} Hz, Fig. 1). For example, in the lowest energy range, nuclei have energy levels associated with their spin with the differences between these energy levels being in the radio frequency range; transitions between spin energy levels of electrons have energy in the microwave region; rotations of molecular groups lie in the far-IR range; molecular vibrations involving stretching and bending of atomic bonds,

have a higher energy, in the mid-IR range; at still higher energies, electronic transitions involving valence electrons are associated with frequencies in the visible range; and those involving inner shell electrons at still higher energies, in the x-ray range. Each of these phenomena in a material can be studied by using incident radiation within a limited frequency range matching the energy of the transitions.

History

Sir William Herschel analyzed in 1800 the distribution of heat in sunlight dispersed through a glass prism. By measuring the temperature of each color he found that the hottest temperature was actually beyond red light. The radiation causing this heating was not visible and Herschel termed this invisible radiation "calorific rays". Today, we know it as infrared. By placing a water-filled container between the prism and the thermometer Herschel discovered, e.g. that water partially absorbs the infrared radiation making his experiments the beginning of **infrared spectroscopy**. On the other hand, **Raman spectroscopy** was "born" more than a century after Herschel's discoveries when the phenomenon of inelastic scattering of light by matter was first observed by Raman and Krishnan (1928). In the original experiment filtered sunlight was focused onto a sample with a second lens collecting the scattered radiation. A system of optical filters was used to show the existence of scattered light with an altered frequency from the incident light – the basic characteristic of Raman spectroscopy.

Basics of Raman and infrared spectroscopy

Vibrational spectroscopy involves the use of light to probe the vibrational behavior of molecular systems, usually via an absorption or a light scattering experiment. Vibrational energies of molecules lie in the approximate energy range 0 – 60 kJ/mol, or 0 – 5000 cm^{-1}. This corresponds to the energy of light in the IR region of the EM spectrum (Fig. 1). As a first approximation, the energy of a molecule can be separated into three additive components associated with *(i)* the motion of the electrons in the molecule, *(ii)* the vibrations of the constituent atoms, and *(iii)* the rotation of the molecule as a whole: $E_{total} = E_{el} + E_{vib} + E_{rot}$. The basis for this separation lies in the fact

that electronic transitions occur on a much shorter time scale, and rotational transitions occur on a much longer time scale, than vibrational transitions.

The energy changes we detect in vibrational spectroscopy are those required to cause nuclear motion. Vibrational transitions can be observed as IR or Raman spectra. However, the physical origins of these two spectra are markedly different. In IR spectroscopy, IR light covering a broad range of frequencies is directed onto the sample. Absorption occurs where the frequency of the incident radiation matches that of a vibration so that the molecule is promoted from the electronic ground level to a vibrational excited state (Fig. 2). The loss of this frequency of radiation from the beam after it passes through the sample is then detected. From the quantum mechanical point of view a vibration is IR active if the dipole moment of the vibrating molecule is changed. It does not matter whether the molecule has a permanent dipole moment or not, only the change associated with the vibration is important.

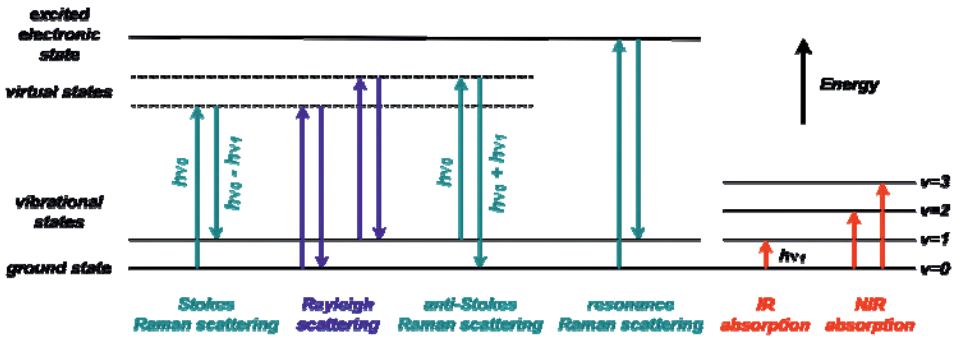

FIGURE 2. Spectroscopic transitions underlying several types of vibrational spectroscopy.

On the other hand, Raman spectra have their origin in the electronic polarization caused by UV, visible or near-IR light. In contrast to IR spectroscopy, Raman spectroscopy uses monochromatic radiation to irradiate the sample and it is the radiation scattered from the molecule, which is detected. Thus, unlike IR absorption, Raman scattering does not require matching of the incident radiation to the energy difference between the ground and excited state. If only electron cloud distortion is involved in scattering, the photons will be scattered with very small frequency changes, as the

electrons are comparatively light. This process is regarded as elastic scattering and is the dominant process (Fig. 2).

For molecules it is called Rayleigh scattering. (Blue light, e.g., is more efficiently scattered than red light, by approx. a factor of n^4, and Rayleigh scattering is responsible for the blue color of the sky.) However, if nuclear motion is induced during the scattering process, energy will be transferred either from the incident photon to the molecule or from the molecule to the scattered photon (Fig. 2). In these cases the process is inelastic and the energy of the scattered photon is different from that of the incident photon by an amount equal to a vibrational transition, $\pm hn_1$. This is Raman scattering. The oscillating electric field of the light interacts with the molecule and polarizes (distorts) the electron cloud around the nuclei to form a short-lived state called a "virtual state" (Fig. 2). This unstable state is not necessarily a true quantum state of the molecule and the photon is quickly re-radiated. Although it is inherently much weaker process than Rayleigh scattering (by a factor of 10^{-3} to 10^{-6}), it is still possible to observe the Raman scattering by using a strong exciting source.

Energy units

According to its wave nature, EM radiation is characterized by two quantities: the wavelength *l* and the frequency *n*. In the IR spectral region the wavelength is usually given in units of [mm]. The frequency is given in units of [s^{-1}] or Hertz [Hz]. The product of *l* and *n* is the velocity of light ($c = ln$), which is approx. $3 \cdot 10^{10}$ cm s^{-1} in vacuum. Since the vibrational frequencies of molecules are so high, units such as Hz are not convenient. An additional parameter, which is commonly used in Raman and IR spectroscopy instead of the frequency, is the *wavenumber,* $\bar{\nu}$, defined as the reciprocal of the wavelength in cm [cm^{-1}]. In general, the energy of the EM radiation is proportional to its frequency and its wave number, but inverse to the wavelength: $E = h\nu = hc\bar{\nu} = hc / l$.

The following relation exists between the wavelength *l*, the frequency *n*, the wavenumber $\bar{\nu}$ and the velocity of light *c*: $\bar{\nu}$[cm^{-1}] = 10^4 / *l* [μm] = *ν* [s^{-1}] / *c* [cm s^{-1}]. Although the dimensions of *n* and $\bar{\nu}$ are different, they are often used interchangeably. Thus, an almost slang expression such as "a frequency shift of 5 cm^{-1}" is very common.

Even though Raman spectroscopy probes vibrational transitions indirectly by light scattering, the Raman shift has the same energy range as IR absorption.

Selection rules

Different vibrational modes have different relative intensities in IR and Raman spectra – some modes are active in one and not the other, and some modes are not observed at all. The IR and Raman activities of particular modes are determined by the quantum mechanical selection rules for the vibrational transitions, and by the mode symmetry. In a simple model, the selection rules can be rationalized by considering the interaction between the oscillating electric field vector of the light beam and a changing molecular dipole moment associated with the vibration. In an IR experiment, the light interacts directly with an oscillating molecular dipole, so for a vibrational mode to be IR active, it must be associated with a changing dipole moment. In general, asymmetric vibrations tend to give stronger IR absorption than symmetric species, since they are associated with larger dipole moment changes. Similarly, highly polar ("more ionic") molecules and crystals have stronger IR spectra than non-polar samples. In Raman scattering, the light beam induces an instantaneous dipole moment in the molecule by deforming its electronic wave function. The atomic nuclei tend to follow the deformed electron positions, and if the nuclear displacement pattern corresponds to that of a molecular vibration, the mode is Raman active. The magnitude of the induced dipole moment is related to the ease with which the electron cloud may be deformed, described by the molecular polarizability a.

The classification of the vibrational quantum states and the description of the spectroscopic interaction are greatly simplified by exploiting the symmetry of the vibrating atomic groups. The mathematical framework of the group theory is the basis of the quantitative description of the symmetry relations possessed by the vibrating groups, finally giving rise to the formulation of the symmetry-based selection rules. As the symmetry of the atomic group increases, the number of different energy levels decreases. The degeneracy, i.e. the number of vibrational states, which have the same energy increases with increasing symmetry. The more symmetric the atomic group, the fewer different energy levels it has, and the greater the degeneracy of those levels. The symmetry must be compatible in order that the molecule may absorb light and the

symmetry-based selection rules tell us which transitions are possible. Thus, the number of allowed transitions in polyatomic molecules is greatly reduced.

Transitions can take place between different vibrational levels (v). The selection rule allows any transitions corresponding to $Dv = \pm 1$ if the molecule is assumed to be a harmonic oscillator. Thus, only the *fundamental normal mode vibrations* that originate in the transition from $v = 0$ to $v = 1$ in the electronic ground state can be observed. *Overtones* (multiples of the fundamental) and *combination bands* (sum or difference of two or more fundamentals) are forbidden. However, they could be observed in the spectra because of the anharmonicity of the vibrations.

The IR portion of the EM spectrum is divided into three regions; near- (NIR), mid- (MIR) and far-IR (FIR), named for their relation to the visible spectrum (Fig. 1). The FIR, ~1-400 cm^{-1} (2000–25 mm), lying adjacent to the microwave region, has low energy and may be also used for rotational spectroscopy. This range covers the vibrational frequencies of fundamental modes (usually weak) associated with metal-oxygen vibrations as well as complex deformations of polymeric units. The MIR, ~400-4000 cm^{-1} (25–2.5 mm), may be used to study fundamental vibrations. The higher energy NIR, ~4000-14000 cm^{-1} (2.5–0.7 mm) can excite overtones or combination vibrations. However, one should keep in mind that such division is somewhat arbitrary.

Light sources

In general, a spectroscopic experiment requires a light source, a means of providing energy resolution of the light before or after interaction with the sample, and a detection system. Since peaks due to Raman scattering are relatively sharp and are measured as a shift from the energy of the excitation source, a monochromatic source is required if quality data is to be obtained. Most Raman spectroscopy is carried out using a laser in the visible region, e.g. 488 nm and 514.5 nm lines of Ar^+ ion laser, 532 nm Nd-YAG solid-state laser, 632.8 nm He-Ne laser, or alternatively using lasers in the UV as well as in the NIR regions, e.g. Kr or Nd-YAG lasers, resp. Various IR sources are used, depending on the wavelength region of interest. Typical light source in laboratory equipment is a ceramic rod “Glo(w)bar” held at high temperature, essentially a "blackbody source". It gives useful intensity between approx. 50 and 10000 cm^{-1}. For FIR studies of silicates, a Globar is usually sufficient, but below ~150 cm^{-1} more

intensity can be obtained from an Hg arc lamp. NIR experiments at wavenumbers greater than ~10000 cm^{-1} require a W filament lamp as source. Synchrotron radiation as a special type of IR source will be briefly introduced in the section *advantages and disadvantages*.

Spectrometers and interferometers

Most modern IR instruments are interferometers, while only a negligible number of grating IR spectrometers and some remainders of prism instruments are still preserved in few laboratories. Fourier transform infrared (FTIR) spectrometers are based on the principle of the Michelson interferometer. Light from the IR source is passed through a 50% reflective beamsplitter, which directs half of the incident intensity to a fixed mirror, and half to a moving mirror. The two beams are recombined at the beamsplitter, so that constructive or destructive interference occurs, depending on the path difference. The result is an interferogram, plotted as light intensity vs. time. For a single frequency source such as laser, the result is a sine wave. This is the Fourier transform (FT) of a delta function at the laser frequency, when intensity is plotted against light energy. In a Fourier transform spectroscopic experiment, light intensity is measured in the time domain, then converted via a FT (using appropriate computer software) to intensity vs. energy (usually expressed in units of wavenumbers, wavelength, or frequency). When the source emits a range of light frequencies, all the resulting sine waves add constructively only when the moving mirror is at the same distance from the beamsplitter as the fixed mirror. Each point of the resulting interferogram contains information over the entire IR region covered by the source. This signal is modified by the particular IR absorbance signature of the sample before reaching the detector. During the FTIR experiment, a reference laser line, usually 632.8 nm He-Ne laser, is also passed through the beamsplitter. The laser signal is monitored by a separate detector, and is used to precisely determine the position of the moving mirror relative to the fixed mirror, and also serves as an internal frequency standard.

To collect Raman scattering effectively it is necessary to remove the much more intense Rayleigh scattering and stray light. The separation of the frequency-shifted Raman scattering and the energy resolution can be done with two or even three monochromators. The purpose of the first monochromator is mainly to separate the

frequency-shifted Raman scattering from the other radiation. The second monochromator increases the dispersion and separates individual Raman peaks. However, filter technology has improved with the development of effective notch and edge filters. The notch filters, in particular, are widely used. They are designed to absorb the light of the frequency of the incident laser light. Usually a filter, which collects most of the light within 200 cm^{-1} of the excitation frequency is regarded as sufficient. Some experiments do require measurements closer to the exciting line and in these cases, the use of monochromators would still be the preferred method for separating the Raman scattering.

FT-Raman was introduced in 1980s. By that time FTIR was developed to a high level of refinement and many components were transferred from FTIR to FT-Raman with minor modifications. Many vendors offer FT-Raman attachments to otherwise conventional FTIR spectrometers, so that both techniques share the same interferometer.

Detectors

There are mainly two classes of IR detectors: thermal and quantum detectors. Thermal detectors detect temperature changes related to the infrared radiation coming from the sample. These detectors have slow response times, but generally have a wide wavelength range of operation. Quantum detectors rely on the interaction of incoming IR photons with the electronic wavefunction of the solid detector material. These detectors have fast response times, but only cover narrow wavelength ranges. Many IR detectors have been developed to operate optimally at liquid-N_2 or liquid-He temperatures, thus reducing the noise from the thermal IR background found even at room temperature. Typical detectors in the MIR range are TGS (triglycin sulphate) or MCT (mercury cadmium telluride). For FIR work TGS is often used despite their low sensitivity. Liquid-He-cooled bolometers with Si or Ge elements cover the FIR with a hundred-fold increase of sensitivity. The main disadvantages of these detectors are their cost and the need of handling liquid-He as coolant. For the NIR liquid-N_2-cooled InAs or InSb detectors are available. Recent developments include two-dimensional arrays of e.g. MCT or bolometer detectors for IR imaging.

In Raman spectroscopy single-channel detectors (photomultipliers and semiconductor photodiodes) are now only employed in scanning, dispersive

spectrometers with special requirements such as access to the very low frequency region as well as in interferometric instruments working in the NIR region. The multichannel solid-state detectors tend now to predominate in micro-Raman systems, either for spectral analysis or Raman imaging. Most of these detectors are based on silicon technology and thus are sensitive to photon energies from the near-UV, ~280 nm, to ~1 μm in the NIR region. Other devices are based on different semiconductors such as Ge or InGaAs whose response extend further into the NIR region.

Microscopy

Raman and IR microscopes developed independently over the past 30 years. The development of both was motivated by the need for acquiring spectra from microspots. Raman microbeam techniques found applications in the earth sciences already in the 1970s. The spatial resolution is determined by physics based on the wavelength of the light used. For Raman in which the wavelengths of excitation and detection are done in the visible range, typically between 400 and 850 nm, the spatial resolution, which is diffraction limited is observed to be better than 1 μm. In micro-Raman spectroscopy, the incident laser beam is directed into an optical microscope and focused through the objective onto the sample. The scattered light is collected back through the same objective (~180º geometry), and sent into the spectrometer. The focus of the incident beam forms an approximate cylinder, whose dimensions are dictated by the wavelength of the laser light and the optical characteristics of the objective and the sample. The diameter of the cylinder is fixed by the diffraction limit of light in air, and is ~0.5-1 μm for an objective with numerical aperture (NA) ~0.9 and laser light in the blue-green region of the spectrum. Corresponding to this is a depth (length) of the scattering cylinder of ~3 μm. This shows that micro-Raman spectroscopy has better lateral resolution than depth spatial resolution. The depth resolution is greatly improved in recently widely employed confocal systems, but is still the less resolved direction. Exact optical conjugation onto the sample of the pinhole apertures, employed for both illumination and detection, rejects the stray light background due to the out-of-focus regions of the specimen. Thus the main contribution to the signal comes selectively from a thin layer close to the focal plane.

Modern developments in IR spectroscopy include the application of the IR technique

to microsamples (down to diameters of 20-50 μm) using IR microscopes. Two types of IR microscopes are available: one based on lenses and the other based on reflecting optics. The reflecting mirror objectives (Cassegrain or Schwarzschild optics) have the advantages to work in the whole IR spectral range. Both have intrinsic limits on the area sampled. If the size of the sample approaches the wavelength of the infrared radiation used, the incident beam is diffracted. For the MIR, the wavelengths are typically between 25–2.5 mm (400-4000 cm-1), which puts the spatial resolution at best at ~5 μm, but more typically at 10–20 μm. To measure FIR spectra, e.g. down to 100 cm-1, sample size must exceed 100 μm. Although IR is still the most widely used vibrational spectroscopy in both research and application labs, in contrast to micro-Raman spectroscopy, micro sampling in the IR is just starting to become popular in the geosciences. While IR microscopes are generally well-suited for mapping purposes using motorized XYZ stages, modern equipment also provide the possibility of area-sensitive detectors that allow for true spectroscopic imaging with high spatial resolution. As for micro-Raman, confocal geometry is employed in modern IR microscopes leading to a significant improvement in the 3D spatial resolution and image contrast.

Advantages and disadvantages

It is obvious even from this brief introduction that the details of every experiment like sample preparation, instrumentation utilized and experimental geometry should be matched to the problem to be solved. Thorough discussion of pros and contras of the different methods is far beyond the scope of this article. Nevertheless, few considerations regarding sources and spectrometers, which could be useful for the choice of instrumentation, will be discussed below.

Light sources: In Raman spectroscopy the choice of laser wavelength usually involves trade-offs among three factors: Raman cross-section, detector sensitivity, and fluorescence. The Raman cross-section decreases with increasing laser wavelength and shorter laser wavelength will yield larger cross-section with a $1/l^4$ dependence. In addition, shorter wavelengths can usually be detected with higher quantum efficiency and less noise, thus improving sensitivity. However, shorter wavelengths are also more likely to excite fluorescence since more electronic transitions occur in the UV and visible than in the IR regions. If a significant number of potentially fluorescent samples

is anticipated, the laser wavelength should be as long as permitted by sensitivity requirements. So, one is trading off the higher sensitivity at shorter laser wavelengths vs. the lower background at longer wavelengths, with the ultimate objective being maximum signal-to-noise ratio.

While modern IR microscopes are designed to work at the diffraction limit, the constraints for the sample size in the case of conventional IR microspectroscopy (> 20 mm) are considerably larger than those for micro-Raman, but even more importantly, larger than the principal limitation by physics. This limit is caused by poor signal-to-noise ratio in IR microscopes with conventional globar light sources due to the low brilliance (also called brightness) of the thermal infrared source. The utilization of synchrotron-based radiation (SR) allows for IR measurements at a diffraction-limited micro-focus, which becomes increasingly important for the characterization of complex samples on the micro- and even on the nano-scale level. As an infrared source, synchrotron radiation has five major advantages compared to conventional laboratory sources: *(i) higher brilliance*: as it is almost a point source, one can focus the light to a diffraction limited size (gain up to 1000x); *(ii) broader spectral range*: continuous from FIR to the visible; *(iii) higher photon flux in the FIR*; *(iv) intense coherent emission* in the lower energy part of the FIR: gain up to 10^5 compared to incoherent SR; *(v) pulsed source* in the ns range: the light is emitted from electron bunches which allows fast timing measurements. There are several high brilliance infrared sources, e.g., synchrotrons, lasers, free-electron lasers (FELs), but of these only the synchrotron provides a ‘‘white’’ source spanning the entire infrared range and is compatible with efficient FTIR techniques.

Spectrometers: while in earth sciences IR spectroscopy is nowadays dominated by the use of FT spectrometers and there is currently no better choice, in Raman spectroscopy the question is dispersive or nondispersive (FT) spectrometer. Dispersive/CCD systems are quite sensitive, laser wavelength can be between ~200 – 800 nm (limited by CCD response), and they use lower laser power. Disadvantages could be the spectral coverage/resolution trade-off and fluorescence. FT-Raman has an excellent frequency precision and better fluorescence avoidance (laser wavelength ≥1064 nm), but the laser power used is often higher. Since the current separation (wavelength availability) is

technical rather than fundamental, it may change with evolving technology. With today's technology, a spectrometer with a laser wavelength longer than 850 nm will be FT, since suitable multichannel detectors are not available for Raman-shifted wavelengths longer than ~1000 nm. Furthermore, there are good reasons (in general) to avoid laser wavelengths <850 nm with a nondispersive system due to the multiplex disadvantage.

In general, spectrometers differ significantly in their ability to observe IR bands or Raman shifts below ~300 cm^{-1} due to the difficulties related to accepting, propagating and detecting long FIR wavelengths and due to the methods used to reject stray laser light, respectively.

Applications of Raman and Infrared spectroscopy

Nowadays mineral spectroscopy has become such an exciting field and applications of Raman and IR spectroscopy in mineralogy and geochemistry are so manifold that it is clearly not possible to do justice to all of this research activity in the scope of this brief article. In the following section, specific aspects of different techniques and instrumentation will be highlighted on the basis of few examples of the use of Raman and IR spectroscopy in mineralogy and geochemistry.

As mentioned above, vibrational spectroscopy measures the vibrational frequencies of interatomic bonds. These frequencies depend on the masses of the atoms involved in the vibration (i.e. on their elemental identity), on the strengths of the bonds (force constants), and on the bond lengths and angles - in other words, on all the parameters that constitute the structure of a molecule or crystal. To identify the vibrations that give rise to features in IR and Raman spectra, we can be guided by a number of qualitative considerations. For example, lighter atoms will vibrate at higher frequencies than heavier atoms, if their bonding is of similar strength; higher bond strengths, usually associated with higher valencies or greater covalency lead to higher bond-stretching frequencies; in covalent structures, bond-stretching vibrations lie at frequencies higher than bond-bending deformations. If single crystals are available, the symmetries of IR and Raman active vibrational modes can be deduced from polarized spectroscopic experiments with the help of factor-group analysis. Since the set of vibrational modes is a characteristic *fingerprint* of the chemistry and structure of the molecular groups in a sample, IR (and

increasingly Raman) spectroscopy is widely applied for routine identification of materials, without necessarily knowing the structural origin of the individual spectral peaks. In some cases there are significant advantages over diffraction methods, as the spectra are easy to obtain from solids, liquids and gases, and from materials with low atomic weight. In earth sciences, vibrational spectroscopy is commonly used to identify specific molecular groups (or to monitor their changes in diverse *in-situ* reactions) such as OH, H_2O, CO_2, CO_3, SO_4, NO_3, SiO_4, CrO_4, CH_2, CH_3, CH_4, etc., all of which usually give intense Raman and IR peaks. Structural changes can be monitored in time-resolved experiments, and the distribution of species in heterogeneous samples can be investigated by mapping and imaging.

Fingerprint analysis in fluid inclusions studies

Fluid inclusion (FI) research, for example, is a worth mentioning field of geochemistry, which greatly benefits from these abilities. Studies of FI provide insights into geological processes in the Earth's crust governed by chemical reactions between rocks and natural fluids. Raman and IR microspectroscopy provide qualitative and quantitative information on molecular species. Sometimes H_2O and OH may cause interferences in the IR analysis of aqueous and gas inclusions due to their strong absorption. On the other hand Raman spectra can be completely obscured by fluorescence emission from inclusions, host minerals, or organics present in the sample or in the mounting media. Molecular components like N_2 (only Raman active), CO_2, CH_4, H_2O and molecular ions such as OH^-, HS^- or SO_4^{2-} can be routinely analyzed in fluid inclusions by Raman and IR spectroscopy. The spectrum in Fig. 3 contains prominent Raman peaks of CH_4 and CO_2 with a trace of N_2 and possibly of H_2S. Other features are bands of the quartz host mineral and cosmic ray spikes.

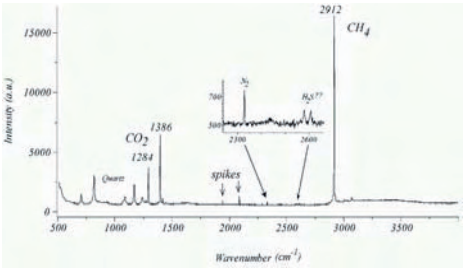

FIGURE 3. Raman spectrum of the vapor phase of aqueous inclusion in quartz (from Samson et al.. 2003).

Hydrocarbon (HC) inclusions are common in petroleum reservoirs and may be considered as fossil oils, which have preserved the original oil composition. Diagenetic minerals generally contain small fluid inclusions (often <15µm) or multi-phase inclusions and it is essential that they are studied individually at the microscale. FTIR is inherently very sensitive to HC, H_2O, etc. but conventional IR microscopes have an unfavorable trade-off between the brilliance of the IR source and the size of the analyzed spot. Fig. 4 presents IR spectra from three different phases in HC inclusion in CaF_2. The oil inside the FI was modified by water impact. To resolve the three phases the measurements were taken at 4 µm spot using the high-brilliance synchrotron IR radiation (SR-IR) at the ANKA light source.

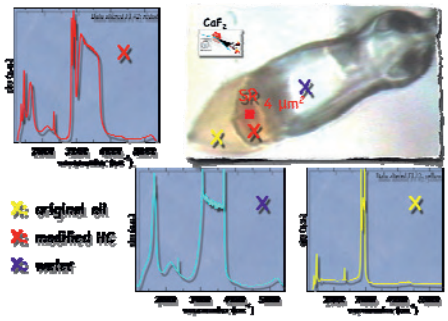

FIGURE 4. IR spectra of the three phases present in HC/aqueous inclusion from Baluchistan.

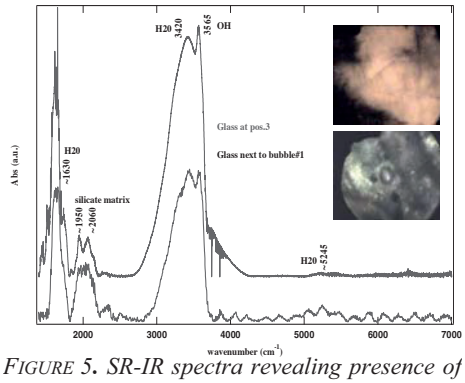

FIGURE 5. SR-IR spectra revealing presence of molecular H_2O as well as OH in two different positions in the silicate matrix of the Bencubbin meteorite.

High-brilliant SR-IR facilitated detection of H_2O inside bubbles in primitive meteorites (Guilhaumou et al., 2005). These meteorites contain high amount of nitrogen, as detected by Raman spectroscopy, which is concentrated mainly as molecular N_2 in relatively large bubbles (20-50 µm) exsolved in some glass phases. SR-IR studies at ANKA have shown that water is also present in detectable quantities inside the bubbles and in some of the glass phases (Fig. 5).

Quantitative analysis, IR mapping and imaging

A further example of use of SR-IR involves the study of water in nominally anhydrous minerals, which in the last two decades has become a “hot topic” in mineralogy, geochemistry and geophysics. Nominally anhydrous minerals (NAMs)

constitute the main reservoir for water in the Earth's mantle. Even traces of water in minerals such as olivine drastically reduce mechanical strength, with major consequences for mantle convection and the formation of minerals as diamonds. The distribution of H_2O around inclusions and cracks in nominally anhydrous mantle minerals such as olivine is studied by IR microspectroscopy mapping (Fig. 6, Sommer et al., 2008).

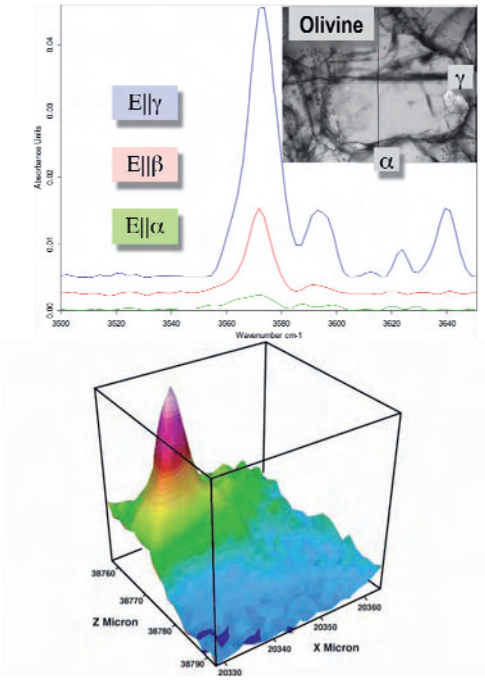

FIGURE 6. Left: Synchrotron IR spectra of OH stretching bands of olivine in α, β, γ directions. The quantitative analysis of anisotropic minerals involves summing absorption intensities from polarized spectra. The water content was calculated with the help of the Beer–Lambert law and a calibration after Bell et al. (2003). The absorbance was normalized to 1 cm sample thickness. The water content (normalized in ppm H_2O by weight) is 138 ppm in the clear, inclusion-free olivine matrix. Right: 3D graph (40x40 μm^2) showing the increase of water towards a totally embedded Cr-spinel inclusion (5-8 μm in size) in olivine. The H_2O content significantly increases towards the inclusion up to values of about 800 ppm.

Large number of overlapping spots was analyzed in a confocal geometry using apertures of 4 or 6 μm and a step size of 2 μm in a grid pattern accessed by an automated stage. The brilliant synchrotron IR light of ANKA is providing the required high spatial resolution. The results show that for all three types of defects in the olivine matrix, i.e. cracks, grain boundaries and Cr-spinel inclusions, the water content increases systematically by a factor of 5–10 towards the defect. Similarly, the defects are all surrounded by halos of water, which increases towards the defects. The data are used to derive passage of aqueous fluids through the lithosphere thus obtaining more detailed information about the ascent rates of kimberlitic melts and their potential for diamond deposits.

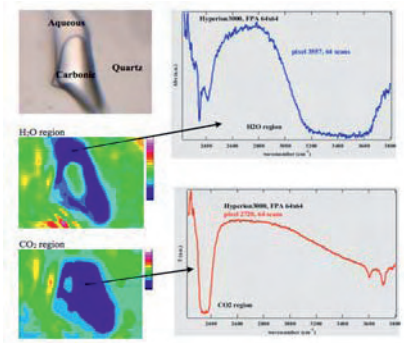

FIGURE 7. IR images of a CO_2-H_2O FI with the corresponding H_2O and CO_2 spectra as extracted from a single pixel of the FPA.

Step-by-step mapping in a confocal arrangement, as shown in the previous example, provides the best spatial resolution and image contrast. The severely reduced flux on the detector at sampling size approaching (or even smaller) than the diffraction limit can be compensated by the high brilliance of the SR-IR. One disadvantage that remains is the long time required to scan the sample (e.g. the sample area shown in the map in Fig. 6, right, was scanned in ~10 h). Much faster one-shot images can be acquired using a multielement focal plane array (FPA) detector. One such study carried out at ANKA involved imaging with a 64 x 64 pixel FPA detector (Fig. 7, Moss et al., 2008). Each pixel in these images corresponds nominally to 1.15 μm^2 on the sample. The time for this experiment was less than 5 minutes! ANKA was the first to demonstrate the value of such multielement detectors at synchrotron IR beamlines (Moss et al., 2006), and this work has proved highly influential, leading to many beamlines worldwide acquiring such detectors. One should keep in mind that this is an apertureless technique and the true spatial resolution as well as the image contrast are deteriorated by diffraction and scattering.

Structural studies: biominerals

Structural changes and dehydration of water/OH containing (bio)minerals could be monitored usually very well by vibrational spectroscopy. In a study by Klocke et al. (2006) thick sections of extracted human teeth were irradiated by CO_2-laser to simulate teeth treatment under different laser operational modes. Raman and IR microspectroscopy were the methods of choice, since the aim was to analyze the gradient of structural alteration and molecular exchange across the CO_2-laser irradiated areas in the dental enamel. The IR absorption spectra were measured with an IR microscope equipped with Ge-ATR objective, for the samples were too thick to observe first-order phonons in transmission geometry. The IR spectra in Fig. 8 indicate loss of water (broad stretching band at 3232 cm^{-1} and the bending band at 1649 cm^{-1}) and OH (sharp peak at 3570 cm^{-1}) as a function of distance from the center of the CO_2-laser spot after irradiation of human dental enamel (outside (curves *a*), at the periphery (curves *b*) and inside (curves *c*) the laser spot. The IR spectra in Fig. 8 show as a function of distance from the center of the CO_2-laser spot a decomposition of CO_3 groups present in the apatite structure (bands around 1400-1550 cm^{-1}), their consequent transformation into CO_2 groups (bands at 2343 cm^{-1}) and their final disappearance in the center of the laser spot. For samples E(1|5|c), those irradiated in a CW laser mode, the CO_3-CO_2 conversion is accompanied by rearrangement of the CO_3 groups in the apatite crystal structure. As the IR absorption at 1412 and 1547 cm^{-1} is associated with CO_3 groups substituting for PO_4 (so-called B-type CO_3) and for OH (A-type CO_3), resp., the observed change in the relative intensities represents a relative decrease of the amount of B-type and an increase of the amount of A-type CO_3 groups. Comparison between the structural changes in the enamel apatite observed in this study to those in heated samples revealed that under laser treatment the achieved average temperature in the center and near the CO_2-laser crater was about 1100 and 700 K, resp. The most intense Raman peak at ~963 cm^{-1} arises from the symmetric stretching mode of PO_4 groups. Its broadening and the appearance of many additional shoulders after irradiation indicates, e.g. variations in the P-O bond lengths and it is evident for structural amorphization.

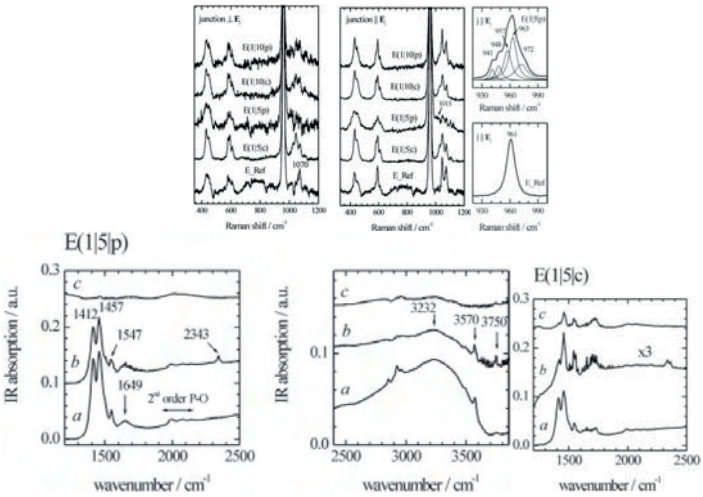

FIGURE 8. Raman scattering and ATR IR spectra of CO_2-laser-treated human dental enamel (consisting mainly of hydroxyapatite, 12% water and 3% organics). After Klocke et al., 2006.

In the IR spectra from inside the laser spot of the samples treated in super pulse laser mode (E(1|5|p, curve *c*) the second order P-O absorption peaks are poorly resolved, which gives further evidence for a lowering of the degree of crystallinity, confirming the Raman results. The smearing of the C-H stretching bands around 2900 cm^{-1} (IR) indicates an impact of the laser treatment on the organics. Increased intensity of the IR band at 3750 cm^{-1} (surface OH groups) is a sign of grain size reduction under irradiation.

Silicates: Silicates are mineralogically and geochemically very important as well crystallographically very exciting class of minerals. In their complex mineral structures, "molecular groups" are not always readily identifiable, especially where the structure is strongly bonded in two or three dimensions. An isolated SiO_4 group (or any tetrahedral XY_4 group) would have nine internal degrees of freedom but only four modes of vibration due to degeneracy (Fig. 9). In structures with isolated SiO_4 tetrahedra it is a very useful starting point to consider the vibrational modes of SiO_4 tetrahedron. The SiO_4 stretching modes are in the high frequency range: n_1 symmetric and n_3 asymmetric stretch ~800-1100

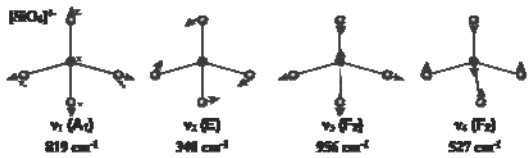

FIGURE 9. Normal modes of vibration of tetrahedral molecules and vibrational frequencies of isolated SiO_4 tetrahedra (Nakamoto, 1997).

cm^{-1}, while the SiO_4 bending modes have a lower frequency: n_2 symmetric and n_4 antisymmetric bend ~300-650 cm^{-1}.

The rules $n_3 > n_1$ and $n_4 > n_2$ hold for the majority of the compounds with isolated SiO_4 tetrahedra. It should be noted that n_2 and n_4 are often too close to be observed as separate bands in Raman spectra. The polymerization of SiO_4 groups to form complex chain anions has important effects on the spectra. For example, the degeneracy of the n_2, n_3 and n_4 modes is lifted, causing the spectrum to become more complex. This is a reflection of the differences of the bonding of the terminal (non-bridging, O_{non}) and bridging (O_{br}) oxygens, which result in different force constants for the Si-O_{non} and Si-O_{br} bonds. Second, a new type of bands attributable to deformation of the Si-O-Si linkage appears in the 550-750 cm^{-1} region, at position(s) depending on the Si-O-Si angle(s), e.g. Lajzerowicz (1966). Thus the effect of polymerization into chains is to split into several components those bands, which occur in the spectra of orthosilicates, and to introduce new bands, which reflect variations in Si-O-Si angle. In practice, Si-O_{non} stretching bands appear in the 950-1200 cm^{-1} region while Si-O-Si bending bands between 550 and 750 cm^{-1}, on the high- and low-frequency sides of the orthosilicate bands at 800-950 cm^{-1}. The vibrations of the cations, which link the complex silicate anions occur ≤400 cm^{-1}. The low frequency compared with the silicate bands reflects the higher coordination number (usually 6-8), the longer metal-oxygen distances, and the lower formal charge (usually 1-3). Taking the symmetric stretching frequency of an AlO_6 octahedron as ~600 cm^{-1}, comparable frequencies for MgO_6, CaO_8, and NaO_8 are calculated as ~470, ~380 and ~270 cm^{-1}, respectively.

Structural studies: poorly crystalline phases

The structure of poorly crystalline calcium-silicate-hydrates (C-S-H) is still a controversial issue, although these materials are extremely important in cement mineralogy. One important aspect in C-S-H structural studies is the degree of polymerization of the silicate units. Its study is a challenging issue due to the poor structural ordering of C-S-H. Therefore, methods not dependent upon long-range structural order are well suited. Raman and IR spectra of series of C-S-H samples with different CaO/SiO_2 ratios (Ca/Si) reveal changes in structure dependent upon Ca/Si ratio (Garbev et al., 2007; Gasharova et al., 2006). Because of the low electronegativity of Ca

a minimal coupling between vibrations involving Ca with those arising from the silicate anionic structure is assumed. This allows the identification of the internal vibrations of the silicate anions. Finite silicate chains (Q^2) dominate the structures of the samples at Ca/Si ratios 0.2-1.0, the spectra showing characteristic symmetric stretching (SS) bands between 1010 and 1020 cm^{-1} (Raman, Fig. 10) and antisymmetric stretching (ASS) ~965 cm^{-1} (IR, Fig. 10). The main characteristic feature of the Raman spectra is the Si-O-Si symmetric bending (SB) vibration at ~670 cm^{-1}. Comparisons with bending frequencies of some known crystalline phases composed of single silicate chains has led to an estimation of the mean Si-O-Si angles in the C-S-H phases to be ~140°, which is the energetically favored bond angle (Garbev et al., 2007). The shift of the SB vibration to a higher frequency (668-672 cm^{-1}, Raman) indicates narrowing of the Si-O_{br}-Si angle with silicate depolymerization. For Ca/Si>1, silicate depolymerization occurs and dimeric silicate units are formed witnessed further in the IR spectra by the increasing intensity of the SS vibration of Si-O Q^1 units ~806 cm^{-1} and the increased splitting of the n_2/n_4 SiO_4 bending around 470 cm^{-1} with increasing Ca/Si ratio. Considering the frequency, intensity, and width of the Raman stretching vibration bands of Q^1 and Q^2 silicate units it was possible to reconstruct some characteristic structural features, such as the chain length of the silicate species as a function of the Ca/Si ratio. The variation in the frequency of the broad OH stretching bands for the different samples is also Ca/Si ratio specific thus implying that the role of H_2O in the structure is essential. The broad shoulder around 3245 cm^{-1} in the Raman spectra is assigned to collective in-phase stretching motions of OH involved in a network of hydrogen bonds. On the other hand, the appearance of a relatively well defined peak at ~3565 cm^{-1} in the Raman spectra of Ca/Si 1.33 and 1.5 suggests increasing ordering of Ca-bonded OH groups. Similarly, increased ordering of the Ca environment is seen in the increase and sharpening of the Ca-O bands at 332 cm^{-1} (Raman) and 255 cm^{-1} (IR). The prominent sharp band at 3618 cm^{-1} (Raman) and 3640 cm^{-1} (IR) due to O-H stretching in portlandite, $Ca(OH)_2$, which first appear in the sample with Ca/Si 1.33 (Raman) and 1.5 (IR) point to excess Ca indicating an upper limit for the incorporation of Ca into the C-S-H structure of less than 1.33 (probably ~1.25). Additional OH band at 3740 cm^{-1} in the IR spectra due to surface silanol (Si-)OH groups is indicative for surface charge, which is also Ca/Si dependent.

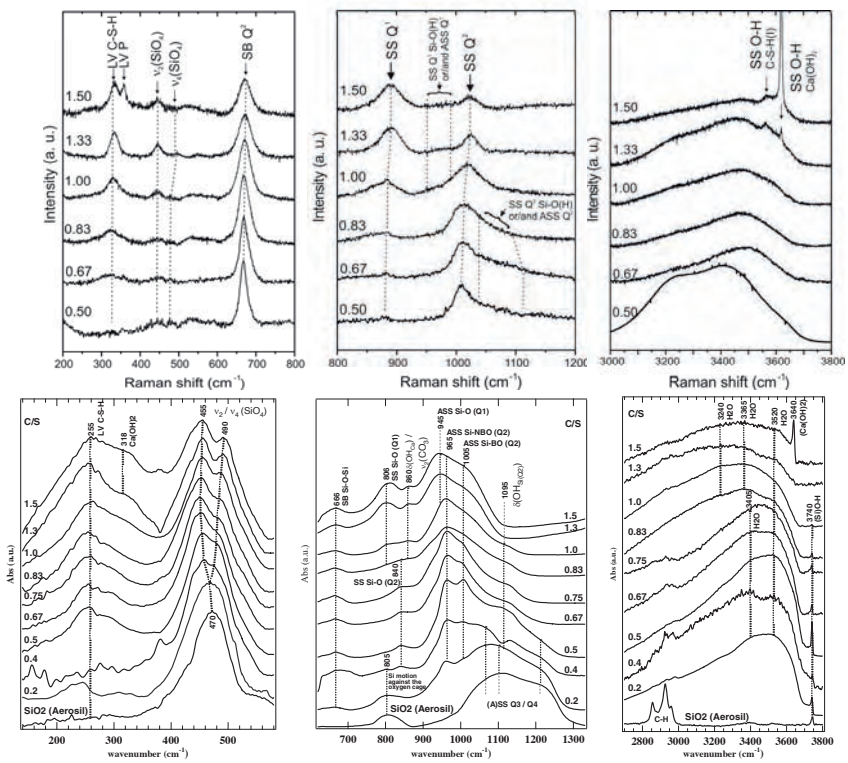

FIGURE 10. The Raman and IR spectra of C-S-H samples of type C-S-H(1) with Ca/Si ratios ranging from 0.2 to 1.5 reveal changes in structure dependent upon Ca/Si ratio.

Surface carbonation of fresh C-S-H samples starts immediately upon exposure to air. The n_1 CO_3 bands overlap with the silicate Raman scattering around ~1080 cm^{-1}. For unambiguous Raman band assignment of C-S-H phases, it is thus imperative to avoid exposure to CO_2, which was assured in the above study by analyzing the samples in sealed quartz glass capillaries. A 40x objective with an adjustable cover-slip correction lens helped minimizing the scattering from the capillary. Further, the effect of carbonation of the same C-S-H samples under ambient conditions for up to 6 months have been investigated by Raman spectroscopy (Black et al., 2007). The technique's sensitivity toward the various $CaCO_3$ polymorphs illuminates the sequence of carbonation and decalcification processes during aging of C-S-H. Amorphous calcium carbonate hydrate is formed within minutes upon exposure to air as indicated by a broad band ~1080 cm^{-1}. It crystallizes, over time, to give primarily vaterite at Ca/Si ≥ 0.67 (e.g.

intense n_1 CO_3 doublet at 1076 and 1091 cm^{-1}; split in-plane n_4 CO_3 bending at 740 and 750 cm^{-1}) and aragonite at Ca/Si ≤ 0.5 (e.g. intense n_1 CO_3 ~ 1080 cm^{-1}; n_4 CO_3 ~700 cm^{-1}). Calcite was not observed as a primary carbonation product within the time frame investigated. Thus, the most probable mechanism of C-S-H carbonation appeared to be of dissolution-precipitation character. Carbonation leads to decalcification of the C-S-H resulting in silicate polymerization (the SB mode at 672 cm^{-1} in the fresh samples sharpened and shifted to 668 cm^{-1} due to polymerization of the Q^1 units).

Structural studies: polarized spectra

As IR activity is dependent on a changing dipole moment, the orientation of the dipole moment change of a given vibration and hence the orientation of a particular bond involved in this vibration relative to the crystallographic crystal axes can be determined, which can give information on the crystal structure and the nature of the vibrational modes. This type of analysis has been particularly useful in the analysis of O-H stretching vibrations in minerals (e.g. Hawthorne, 1988). Synchrotron IR microspectroscopy has been used by Garbev et al. (2008) to study the mechanisms of the phase transformations in the $2CaO\text{-}SiO_2\text{-}H_2O$ system, which understanding has crucial importance for the development of low-energy belite cement materials. The new materials should substitute the common cement clinker produced at 1450°C, with the goal of lowering both the production costs of cement as well as the CO_2 emissions. Part of these studies focus on the dehydration process of α-$Ca_2[SiO_3(OH)](OH)$ (α-C_2SH) because it transforms into hydraulic Ca_2SiO_4 polymorphs at temperatures much lower than 1450°C. Although often studied the structure of α-C_2SH and the mechanism of its dehydration have been not fully resolved. IR studies of α-C_2SH single crystals were carried out under the IR microscope at the ANKA-IR beamline. The brilliance of SR-IR allowed the selection of untwined and homogeneous areas. Study of polarized IR spectra of α-C_2SH contributes to the refinement of its crystal

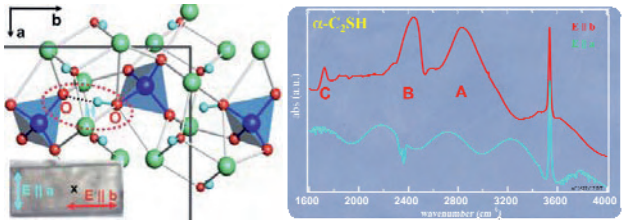

FIGURE 11. OH stretching of OH involved in strong H-bonding in α-C_2SH. (Garbev et al., in prep.).

structure. For example, when the orientation of the electric field vector (**E**) is set to be parallel to the crystallographic *b* axis (**E** || *b,* Fig. 11) three bands are observed between 1600 and 3000 cm^{-1} typical for OH stretching of hydroxyl involved in strong hydrogen bonding. They are denoted C (1715 cm^{-1}), B (2380 cm^{-1}, very broad), and A (2780 cm^{-1}, very broad). Rotating the crystal by 90º (**E** || *a*) leads to disappearance of these bands. This observation not only proves the existence of hydroxylated $SiO_3(OH)$ tetrahedra in the α-C_2SH structure, but also suggests that they are interconnected in a chain-like pattern by H-bonds with orientation along the *b* axis (Fig. 11, right). Studies between 18 and 470 K in a liquid-He cryostat under the IR microscope suggest that the hydrogen bonds are triggering the phase transformation reactions of α-C_2SH upon thermal treatment (Garbev et al., in prep.).

RAIR studies of thin films

Vibrational spectroscopy has great advantages over other techniques such as x-ray diffraction (XRD) and even synchrotron XRD in detecting crystalline particles with a size of just a few unit cells. In addition, the vibrational spectra can unambiguously distinguish between amorphous and crystalline features, which are sometimes a problem for other surface-sensitive spectroscopic methods. In a recent experiment at the IR beamline at ANKA it has been shown that RAIR experiments in grazing incidence geometry are very suitable to examine the efficiency of synthesis methods for ultrathin zeolite film growth (Tosheva et al., submitted). The ultrathin films were transferred to Au coated slides and the spectra were collected using p-polarized light. The enhancement of the IR absorption due to the presence of a strongly reflecting noble metal surface allows the detection of even monomolecular layers when grazing-incident RAIR spectroscopy is used. The utilization of the synchrotron IR source ensured the acquisition of highest quality RAIR spectra due to the natural collimation of the beam.

Overcoming the diffraction limit: near-field Raman and IR nanospectroscopy

The possibility to measure samples at a nano-scale spatial resolution with Raman and even with infrared radiation will soon become a further attraction for mineralogists. Near-field Raman and IR spectroscopy (also called tip-enhanced spectroscopy) will be briefly introduced during the oral presentation.

References

Beran A. and Libowitzky E., Eds. (2004). European Mineralogical Union, Notes in Mineralogy, Eötvös University Press, Budapest.

Burns R.G. and Greaves C. (1971). Amer. Mineral., 56, 2010-2025.

Black L., Garbev K., Gasharova B., Breen C., Yarwood C., Stemmermann P. (2007). J. Am. Ceram. Soc., 90, 908-917.

Chalmers J. and Griffiths P., Eds. (2001). Handbook of vibrational spectroscopy, John Wiley & Sons, Inc.

Garbev K., Gasharova B., Bernotat-Wulf H. and Stemmermann, P. (2005). FZKA Nachrichten, 37, 235-241.

Garbev K., Gasharova B., Beuchle G., Kreisz S. and Stemmermann P. (2008). J. Am. Ceram. Soc., 91, 263–271.

Garbev K., Gasharova B., Black L., Breen C., Yarwood C., Stemmermann P. (2007). J. Am. Ceram. Soc., 90, 900-907.

Gasharova B., Garbev K., Bornefeld M., Black L. and Stemmermann P. (2006). Acta Crystallographica, A62, 208. Leuven, Belgium.

Guilhaumou N., Gasharova B., Mathis Y.-L., Perron C. and Fieni C. (2005). ANKA annual report.

Farmer V.C., Ed. (1974). The infrared spectra of minerals. Mineralogical society, monograph, 4.

Hawthorne F.C., Ed. (1988). Spectroscopic methods in mineralogy and geology. Reviews in mineralogy, Vol. 18.

Klocke A., Mihailova B., Zhang S., Gasharova B., Stosch R., Güttler B. Kahl-Nieke, B., Henriot P., Ritschel B., Bismayer U. (2006). Journal of Biomedical Materials Research Part B: Applied Biomaterials, 81B, 499-507.

Lajzerowicz J. (1966). Acta Crystallographica, 30, 357-363.

McCreery R.L. (2000). Chemical analysis, Vol. 157. John Wiley & Sons, Inc.

Mirabella F.M., Jr., Ed. (1992). Practical spectroscopy series, Vol. 15, Marcel Decker, Inc.

Moss D.A., Gasharova B., Mathis Y.-L. (2008). Synchrotron Radiation News, 21, 51-59.

Moss, D.A., Gasharova, B., and Mathis, Y.-L. (2006). Infrared Phys. Techn., 49, 53-56.

Nakamoto K. (1997) Infrared and Raman spectra of inorganic and coordination compounds, 5th edition, John Wiley & Sons, Inc.

Putnis A. (1995) Introduction to mineral sciences. Cambridge University Press.

Raman C.V. and Krishnan K.S. (1928). Nature, 121, 501.

Samson I., Anderson A., Marshall D., Eds. (2003), Fluid inclusions: analysis and interpretation. Mineralogical association of Canada.

Sommer, H., Regenauer-Lieb, K., Gasharova, B., Siret, D. (2008). Miner. Petrol. DOI 10.1007/s00710-008-0002-9.

Turell G. and Corset J., Eds. (1996), Raman microscopy: Developments and applications. Elsevier Academic Press.